Hindawi Publishing Corporation
Journal of Chemistry
Volume 2016, Article ID 8685437, 11 pages
http://dx.doi.org/10.1155/2016/8685437

Research Article

A Study on Astrazon Black AFDL Dye Adsorption onto Vietnamese Diatomite

Bui Hai Dang Son,[1] Vo Quang Mai,[2] Dang Xuan Du,[2] Nguyen Hai Phong,[1] and Dinh Quang Khieu[1]

[1]*College of Science, Hue University, Hue 530000, Vietnam*
[2]*Faculty of Natural Sciences, Saigon University, Ho Chi Minh City 700000, Vietnam*

Correspondence should be addressed to Dinh Quang Khieu; dqkhieu@hueuni.edu.vn

Received 3 April 2016; Accepted 12 May 2016

Academic Editor: Mohammad A. Al-Ghouti

In the present paper, the adsorption of Astrazon Black AFDL dye onto Vietnamese diatomite has been demonstrated. The diatomite was characterized by XRD, SEM, TEM, EDS, and nitrogen adsorption/desorption isotherms. The results show that diatomite mainly constituted centric type frustules characterized by pores as discs or as cylindrical shapes. The adsorption kinetics and isotherms of dye onto Vietnam diatomite were investigated. The experimental data were fitted well to both Freundlich and Langmuir in the initial concentration range of 400–1400 mg L^{-1}. The average value of maximum adsorption capacity, q_m, calculated from Freundlich equation is statistically similar to the average value of maximum monolayer adsorption capacity calculated from Langmuir equation. The thermodynamic parameters evaluated from the temperature dependent on adsorption isotherms in the range of 303–343 K show that the adsorption process was spontaneous and endothermic. The Webber and pseudo-first/second-order kinetic models were used to analyze the mechanism of adsorption. The piecewise linear regression and Akaike's Information Criterion were used to analyze experimental data. The results show that the dye adsorption onto diatomite was film diffusion controlled and the goodness of fit of experimental data for kinetics modes was dependent on the initial concentration.

1. Introduction

Dyes are a kind of organic compounds with complex aromatic molecular structures that can cause bright and firm color to other materials. However, the complex aromatic molecular structures of dyes make them more stable and more difficult to be biodegraded [1, 2]. Waste water from the textile industry is often strongly colored even for low dye concentrations. In addition, these molecules lead to high chemical oxygen demand, and they exhibit low biodegradability. An important class of molecules is the azo-dyes, which contain nitrogen atoms as azo functional groups [–N=N–] in their chemical structure. They represent half of the dyes used nowadays in the textile industry [2]. Many treatment systems have been proposed for the removal of synthetic dyes from aqueous solution. Methods based on adsorption [3, 4], biological treatments [5], coagulation, electrochemical techniques [6], membrane processes [7, 8], oxidation/ozonation [9, 10], and photochemical oxidation [11, 12] are known to be effective in the removal of this type of dyes from polluted water. Adsorption is considered to be competitive and economically cost effective and efficient process for removal of dyes and heavy metals. Activated carbon is the most employed adsorbent for toxic species removal from aqueous solution because of well-developed pore structures and a high internal surface area that leads to its excellent adsorption properties [13]. However, the high cost of activated carbon and recycle ability sometimes restrict its applicability for dye removal. Therefore, in recent years, a considerable number of studies have investigated into low cost and efficient alternative materials such as clay [14], diatomite [15], and zeolite [16].

Diatomite, a siliceous lightweight sedimentary rock, has received attention for its unique properties including high porosity, small particle size, large surface area, and chemical inertness and as low cost material for the removal of pollutants from waste water. Several studies have been

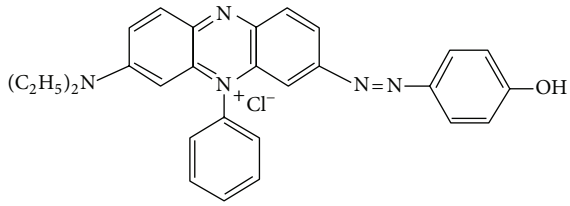

Scheme 1: Structural formulae of Astrazon Black AFDL.

studied on using diatomite as an adsorbent for removing some contaminants such as heavy metals [17], volatile organic compounds (*o*-xylene) [18], basic dyes (methylene blue) [19], and some textile dyes (Red 3BS, Int Yellow 5GF) [20].

In the present paper, the adsorption of AB dye onto Vietnam diatomite has been demonstrated. The adsorption isotherms and kinetics of AB onto diatomite were studied. The thermodynamic data (ΔH^0, ΔS^0, and ΔG^0) are calculated from temperature dependent sorption isotherms and are used to evaluate the sorption properties of dye on raw diatomite. Webber's intraparticle-diffusion model and *pseudo*-first/second-order kinetic models were used to analyze the mechanism of adsorption. AIC and the piecewise linear regression method were used to analyze kinetics data for Webber's intraparticle diffusion model.

2. Experimental

2.1. Materials. Diatomite sample was supplied as a natural resource from Phu Yen province, Vietnam. After removing organic stuff by repeated sedimentation and desiccation at 100°C, the sample was stored in a desiccator for further usage. Sodium hydroxide (NaOH) and hydrochloric acid (HCl, 39%) were purchased from Sigma-Aldrich. Astrazon Black AFDL ($C_{28}H_{28}N_5O$ M = 440 g mol^{-1}) (denoted as AB) was provided kindly from Thuyduong Textural Company (Vietnam). AB is a cationic dye that belongs to azo-dye group. Its structure is shown in Scheme 1.

2.2. Determination of the Point of Zero Charge. The point of zero charge (pH_{PZC}) of diatomite was determined by the solid addition method [21]. To a series of 100 mL flasks, 5 mL of 0.1 M NaCl solution and 40 mL of distilled water were added. The initial pH value (pH_i) of the solution was adjusted from 2.3 to 7.7 by adding either 0.1 M NaOH or 0.1 M HCl. Total volume of solution in each flask was made exactly to 50 mL by adding distilled water. The 0.01 M NaCl solution with different pH value was obtained. Then, 0.1 grams of diatomite was added to each flask and mixtures were stirred for 24 hours; the final pH (pH_f) of solution was measured. The difference between the initial solution and final solution ($\Delta pH = pH_i - pH_f$) was plotted against the pH_i. The point of intersection of curve with abscissa, at which $\Delta pH = 0$, provided pH_{PZC}.

2.3. Isothermal and Thermal Dynamic Studies. For the adsorption isotherm study, add in turn 50, 100, 150, 200, 250, and 300 mg diatomite into 6 stopper 250 mL Erlenmeyer flasks containing 100 mL of AB solution with known concentration (400–1400 mg L^{-1}) and then place them into the shaker bath at 25 ± 1°C for 24 hours. Since initial experiments show that the AB dye/diatomite system reached equilibrium around 120 minutes, the adsorption time was prolonged for 24 hours to ensure saturation. Thereafter supernatant liquid was separated by centrifugation and the final dye concentrations were determined by visible spectrophotometry. A series of isothermal experiments were repeated three times.

The amount of the dye adsorbed by the adsorbents was calculated by the equation:

$$q = \frac{V\left(C_o - C_f\right)}{m}, \tag{1}$$

where q is the amount of dye adsorbed per unit of amount absorbent (mg g^{-1}), C_o is the initial AB concentration (mg L^{-1}), C_f is the dye concentration (mg L^{-1}) after the batch adsorption procedure, V is the volume of dye solution (L), and m is the mass (g) of the adsorbent.

To describe the adsorption isotherms, the Langmuir and Freundlich models were selected for using in this study.

Langmuir isotherm: the Langmuir equation is valid for monolayer sorption onto the surface. Its linear form could be expressed as follows [17, 22]:

$$\frac{1}{q_e} = \frac{1}{K_L q_{\text{mom}}}\frac{1}{C_e} + \frac{1}{q_{\text{mom}}}, \tag{2}$$

where q_{mom} is the maximum monolayer capacity amount (mg g^{-1}), K_L is Langmuir equilibrium constant, q_e is the quantity of AB dye adsorbed per unit of amount absorbent (mg g^{-1}) at equilibrium time, and C_e is the concentration present at equilibrium (mg L^{-1}). The linear plot of $1/q_e$ *versus* $1/C_e$ provides the value of K_L and q_{mom}.

The essential characteristics of Langmuir isotherm can be expressed in terms of a dimensionless constant separation factor, R_L, which is performed as

$$R_L = \frac{1}{\left(1 + C_o K_L\right)}, \tag{3}$$

where the value of R_L indicates the type of isotherm: unfavorable ($R_L > 1$), linear ($R_L = 1$), favorable ($0 < R_L < 1$), or irreversible ($R_L = 0$) [23].

Freundlich isotherm: Freundlich equation is empirical relation based on the sorption onto the heterogeneous surface. Its linear form is commonly represented as [17, 24]

$$\ln q_e = \ln K_F + \frac{1}{n}\ln C_e, \tag{4}$$

where K_F (mg g^{-1}) is the Freundlich constants, which is a measure of adsorption capacity, and $1/n$ is an empirical parameter related to the nature and strength of the adsorption process and the distribution of the active sites. The linear plot of $\ln q_e$ *versus* $\ln C_e$ provides the value of K_F and n. Low values of $1/n$ mean that the surface is heterogeneous. For values in the range $0.1 < 1/n < 1$, adsorption is favorable. Values of $1/n$ between 0.1 and 0.5 represent good adsorption processes,

whereas $0.5 < 1/n < 1$ indicates that adsorption capacity is only slightly suppressed at lower equilibrium concentrations [25].

In order to evaluate whether the adsorption process is spontaneous, the thermodynamic parameters of adsorption are studied. Experimental procedure was conducted as an adsorption isotherm study; however, the temperature of process was fixed at 303, 313, 323, 333, and 343 K. The Gibbs free energy ΔG^0 of adsorption is given by the relation [17]

$$\Delta G^0 = \Delta H^0 - T\Delta S^0, \tag{5}$$

where ΔG is given by Van't Hoff's equation:

$$\begin{aligned} \Delta G^0 &= -RT \ln K_L \\ \ln K_L &= -\frac{\Delta H^0}{RT} + \frac{\Delta S^0}{R}, \end{aligned} \tag{6}$$

where K_L is equilibrium constant equal to Langmuir equilibrium constant. The linear plot of $\ln K_L$ *versus* $1/T$ gives the value of ΔH^0 and ΔS^0.

2.4. Adsorption Kinetics Study. Kinetic studies were carried out in a 3 L plastic beaker. The plastic beaker was equipped with a stainless steel flat blade impeller using an electric motor to stir the dye solution. Diatomite (0.50 g) was mixed thoroughly with 1000 mL of RDB solution in the beaker at room temperature. Ten-millilitre samples were drawn periodically through tap and diatomite was removed by centrifuging process. The final dye concentrations were determined by visible spectrophotometry. The experiments were conducted with various AB concentration in the range of 150–900 ppm. For each concentration, the experiments were repeated three times and the mean value was taken.

In the present paper, two kinetic models and Webber intraparticle-diffusion model were used. The *pseudo*-first-order kinetic model in nonlinear form is Lagergren equation [26, 27] and written as

$$q_t = q_e \left(1 - e^{-k_1 t}\right), \tag{7}$$

where q_t and q_e are the capacity amount of dye adsorbed at time t (min) and at equilibrium time, respectively, and k_1 is rate constant of *pseudo*-first-order equation (min^{-1}). k_1 and q_e were calculated by nonlinear regression method.

And the *pseudo*-second-order kinetic model in nonlinear form was expressed as follows [28, 29]:

$$q_t = q_e \frac{q_e k_2 t}{1 + q_e k_2 t}, \tag{8}$$

where k_2 is rate constant of *pseudo*-second-order kinetic equation ($\text{g mg}^{-1}\ \text{min}^{-1}$).

k_1, k_2, and q_e were calculated by nonlinear regression method using Solver function in Microsoft®Excel™.

Webber's intraparticle-diffusion model is described as the following equation [28, 30]:

$$q_t = k_i t^{1/2} + I, \tag{9}$$

Table 1: Chemical composition of diatomite analyzed by EDS.

Oxide	Al_2O_3	SiO_2	TiO_2	Fe_2O_3	Others
% wt	20.72	68.35	0.92	9.21	0.80

where k_i is intraparticle-diffusion rate constant ($\text{mg g}^{-1}\ \text{min}^{-0.5}$) and I is the intercept which represents the thickness of the boundary layer. If intraparticle-diffusion is the rate-limiting step, then a plot of q_t *versus* $t^{0.5}$ will give a straight line with a slope that equals k_i and an intercept equal to zero.

2.5. Characterization of Materials. The powder X-ray diffraction (PXRD) patterns were recorded by a D8 Advance, Bruker, Germany, with CuKα radiation (λ = 1.5406 Å). The morphology and surface composition of diatomite were determined by scanning electron microscope (SEM) and energy dispersive spectroscopy (EDS), respectively, using SEM JMS-5300LV. The textural properties of diatomite were determined by nitrogen adsorption/desorption isotherms using a Micromeritics 2020 volumetric adsorption analyzer system. Fourier transform-infrared (FTIR) measurements were carried out by the KBr method using Shimadzu FTIR 8010M. Visible spectrophotometry was measured by Lambda 25 Spectrophotometer (Perkinelmer, Singapore) at $\lambda_{\max}$ of AB dye (610 nm).

3. Results and Discussion

3.1. Characterization of Diatomite. Figure 1(a) shows the SEM observation and PXRD patterns of diatomite in this study. As observed in Figure 1, the sample of diatomite was mainly formed by centric type frustules which were characterized by notable pores as discs or as cylindrical shapes indicating that there is a good possibility for dyes to be adsorbed into these pores. The chemical analysis by EDS (Table 1) showed that silica represents the major composition (68% wt) and metallic oxides contribute to the rest. PXRD analysis presented in Figure 1(b) indicating that silica occurs under amorphous phase due to very low intensity of PXRD diffraction. The amorphous silica phase is found to be characteristic of the frustule composition as reported in previous studies [30, 31].

FTIR analyses were performed in the range 400–4000 cm^{-1} as shown in Figure 2. The main absorption bands for diatomite were observed at 3695, 3622, 3421, 2858, 1639, 1153, 1022, 914, 798, 690, 528, and 443 cm^{-1}. The bands at 3695, 3622, and 2858 are attributed to the free silanol group (Si–O–H) and the band at 1639 cm^{-1} corresponds to H–O–H bending vibration of water. The bands at 1153 and 1022 are assigned to the siloxane (–Si–O–Si–) group stretching and the 914 cm^{-1} band represents Si–O stretching of silanol group. The 798 and 690 cm^{-1} bands represent SiO–H vibration. The absorption peaks around 528 and 443 cm^{-1} are attributed to the Si–O–Si bending vibration [32–34].

Figure 2(b) shows the nitrogen adsorption/desorption isotherm of diatomite. Diatomite sample exhibited type IV isotherm and a H4-type hysteresis loop indicating the

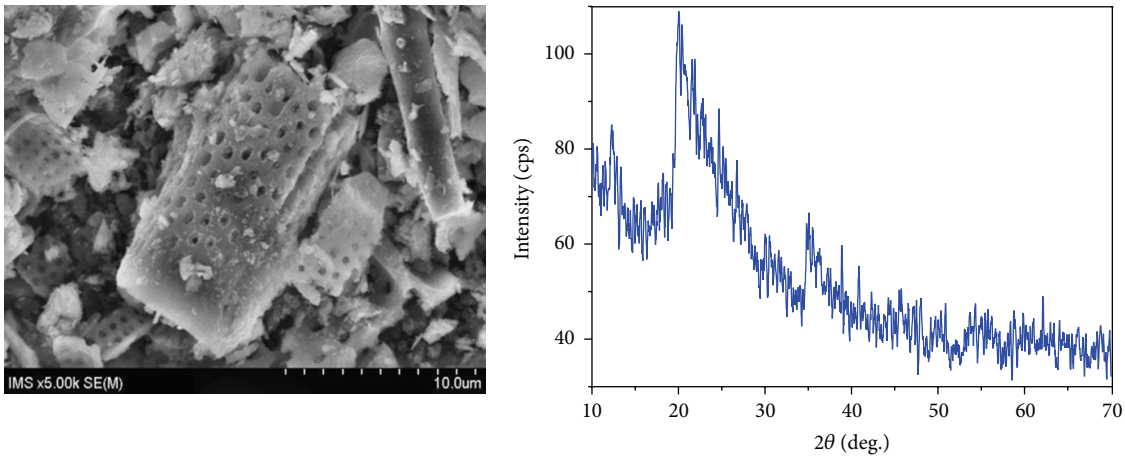

Figure 1: SEM observation (a) and PXRD pattern (b) of diatomite.

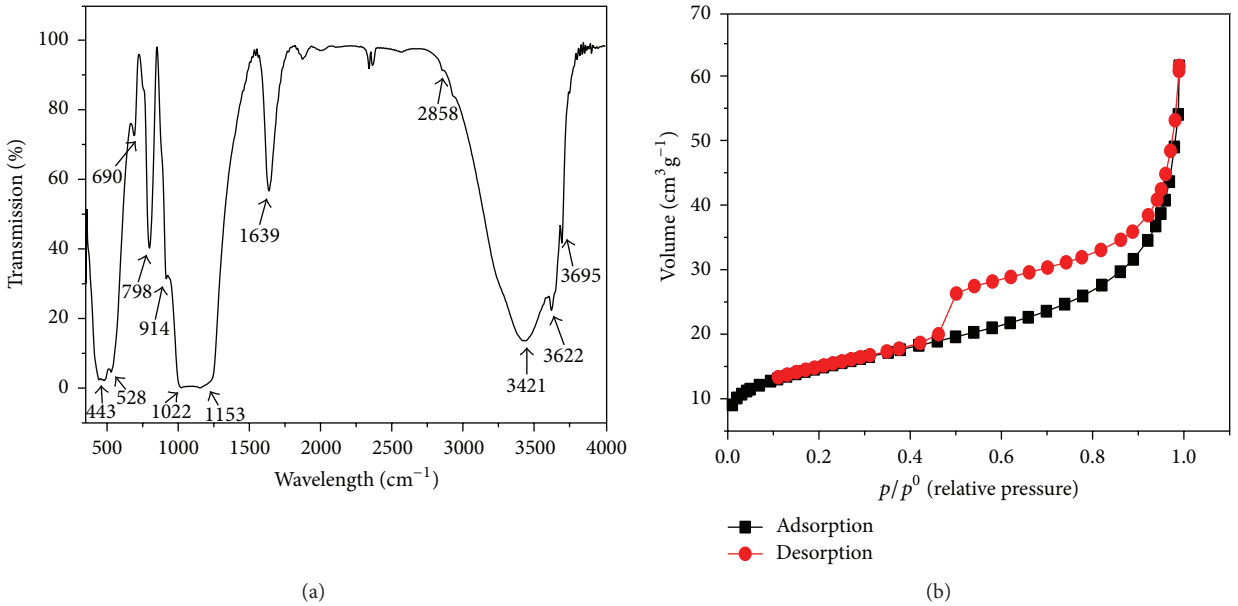

Figure 2: FTIR spectrum (a) and nitrogen adsorption/desorption isotherms (b) of diatomite.

presence of the slit-like pore structure [35]. The diatomite with BET surface area around 51 $m^2\,g^{-1}$ and pore volume of 0.0952 $cm^3\,g^{-1}$ is rather higher than those of reported diatomite [34, 36]. The present diatomite, which is composed of amorphous silica, has properties such as high porosity and high surface area indicating a potential absorbent for adsorption.

3.2. pH Effect of Solution on AB Dye Adsorption. Solution pH has a significant influence on the adsorption process because it can influence both the ionisation of pollutants and the ionic state of the functional groups on the surface of adsorbent. As seen in Figure 3, the adsorption capacity of AB onto diatomite increased with the increase in pH. The equilibrium adsorption capacity, q_e, increased from 80.08 to 98.1 mg g^{-1} as pH of the dye solution increased from 4 to 11. The pH_{ZPC} of diatomite determined by solid addition method is around 5.4 (the inset in Figure 3) which was similar to that of a kind of diatomite as [37]. Thus, it is obvious that the ionisable charge sites on the diatomite surface increased when pH increased from 4 to 11. When the solution pH was below pH_{ZPC}, the diatomite surface had a positive charge, while at high pH (pH > 5.4) it has a negative charge. Hence, when the pH of AB solution increased, the adsorption of AB molecules with positive charge was enhanced as described in

$$\equiv \text{Si–OH} + \text{H}^+ \longrightarrow \equiv \text{Si–O}^- + \text{H}_2\text{O} \quad (10)$$

$$\equiv \text{Si–O}^- + \text{AB}^+ \longrightarrow \equiv \text{Si–O–AB} \quad (11)$$

Table 2: The isotherm parameters of Langmuir and Freundlich models at various concentrations from 400 to 1400 mg L^{-1}.

C (mg L^{-1})	Langmuir model					Freundlich model				
	q_{mom}	K_L	R^2	R_L	p	$1/n$	K_F	q_m	R^2	p
400	357.1	0.0244	0.955	0.0930	0.000	0.429	34.2607	447.3	0.975	0.000
500	416.7	0.0123	0.947	0.1402	0.001	0.480	24.2060	476.5	0.987	0.000
600	526.3	0.0098	0.957	0.1450	0.000	0.478	27.1669	578.8	0.978	0.000
800	625.0	0.0046	0.968	0.2132	0.000	0.499	20.5672	579.0	0.991	0.000
900	666.7	0.0033	0.975	0.2507	0.000	0.494	19.4608	560.1	0.977	0.000
1200	625.0	0.0020	0.986	0.3431	0.000	0.541	22.7250	539.3	0.961	0.001
1400	625.0	0.0021	0.946	0.2528	0.001	0.379	30.7288	477.5	0.931	0.002

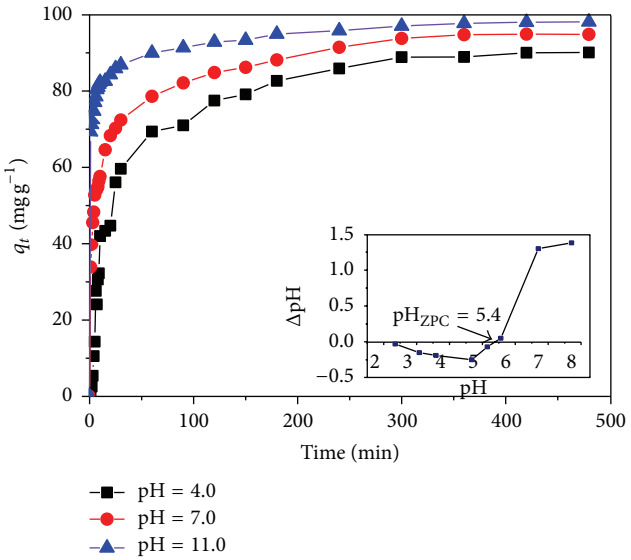

Figure 3: The pH effect on the AB adsorption from aqueous solution by diatomite. Adsorption condition: initial AB concentration = 200 mg L^{-1}, mass of adsorbent = 2.0 g, volume of solution = 1000 mL, and stirring speed = 300 rpm. The plot of ΔpH versus initial pH (inset).

3.3. The Study of Adsorption Isotherm and Thermodynamics. Isotherm studies were conducted to provide information on the capacity of the adsorbents under different concentrations of AB. The equilibrium data were analysed using the Langmuir and Freundlich model. The Langmuir and Freundlich isotherm parameters for AB adsorption onto the diatomite were calculated by plotting of $1/q_e$ *versus* $1/C_e$ and $\ln q_e$ *versus* $\ln C_e$, respectively, and the results are presented in Table 2. The Freundlich equation describes an equilibrium between q_e and C_e and value of q_e increases with an increase in C_e. The maximum adsorption capacity amount is not obtained in Freundlich equation. In the present work, the equilibrium experiments were controlled as if the initial concentration (C_i) was kept constant and the diatomite absorbent was varied from 50; 100; 150; 200; 250; and 300 mg L^{-1}. Halsey [38] supposed that the maximum adsorption capacity, q_m, by Freundlich equation could be expressed

$$q_m = \lim_{C_e \to C_i} K_F C_e^{1/n}, \quad (12)$$

where q_m calculated based on Freundlich equation are also shown in Table 2.

As can be seen in Table 2 both models are very close to coefficients of determination (R^2) and favorable characteristic parameters (i.e., R_L for Langmuir isotherm and $1/n$ for Freundlich isotherm). The value ($0 < R_L < 1$) and the value of $1/n = 0.38$–0.54 in the range 0.1–0.5 indicate both isotherms are favorable. In the statistical view the linear regression between $1/C_e$ *versus* $1/q_e$ and $\ln C_e$ *versus* $\ln q_e$, respectively, does have statistical significance because the value of p is much smaller than the usually accepted 0.05 significance level ($p = 0.000 < \alpha = 0.05$ in all cases) [39]. These results confirmed that the equilibrium data of AB adsorption onto the diatomite could be well fitted by the two adsorption isotherm models. The high correlation to both Langmuir and Freundlich isotherms implies a monolayer adsorption and the existence of heterogeneous surface in the adsorbents, respectively.

For Langmuir model, K_L was known as equilibrium constant which should be constant at specified temperature. q_{mom} is the maximum monolayer adsorption capacity which is thought to be specified for each absorbent. However, the data in Table 2 show that K_L and q_{mom} are not constant at specified temperature but tend to increase as the initial concentration increases. In similar manner, the parameters of Freundlich model were also varied monotonically with the increase in initial concentration in the range of 400–900 mg L^{-1}. As the initial concentration is too high, the large AB aggregates could block the pores of diatomite that result in low adsorption capacity amount. Then, the parameters of models calculated in case of high initial concentration may be uncorrected. In the range of initial concentration from 400 to 900 mg L^{-1}, q_{mom} and q_m are as a function of initial concentration. Pair sample t-test was conducted to compare the difference of q_m and q_{mom}. Since p value is larger than 0.05 significant level the difference between the average value of q_m ($M = 518.0 \pm 13.2$ mg g^{-1}) and the average value of q_{mom} ($M = 528 \pm 62$ mg g^{-1}) is not statistically significant ($t(4) = -0.269$, $p = 0.801$) [38]. It means the value calculated from both isotherm models is statistically similar. The data of maximum adsorption capacity shows that diatomite possesses very high capacity of dye adsorption compared to other minerals as adsorbents [2].

The thermodynamics were studied at 303, 313, 323, 333, and 343 K. At each temperature, K_L were determined

Table 3: Thermodynamic parameters for the adsorption of AB dye on diatomite.

T (K)	$\Delta G_T^0 = \Delta H - T\Delta S^0$ (J mol^{-1})	ΔH^0 (J mol^{-1})	ΔS^0 (J mol^{-1} K^{-1})
303	−21110.85	29778	167.95
313	−22790.35		
323	−24469.85		
333	−26149.35		
343	−27828.85		

through (2) by linear plot of $1/q_e$ and $1/C_e$. The thermodynamic parameters, ΔH^0, ΔG^0, and ΔS^0, of the system were determined using the Van't Hoff equation to evaluate the spontaneity of the adsorption process. The graph of plotting $\ln K_L$ *versus* $1/T$ provided the linear line in statistical view ($F(3) = 223.7$, $p = 0.004 < 0.05$) (see Figure 5).

The thermodynamic parameters are presented in Table 3. The large and positive value of ΔH^0 indicates that adsorption is endothermic process and chemical sorption by nature. The positive value of ΔS^0 indicates the increasing randomness at the solid-liquid interface during the adsorption of AB molecules on the diatomite [40]. The higher the temperature the more the negative values of Gibbs free energy, ΔG^0, for AB adsorption on diatomite, which implies that the spontaneity increases with the increase in the temperature. As the Gibbs free energy change is negative accompanied by the positive standard entropy change, the adsorption reaction is spontaneous with high affinity. Based on the values of ΔH [41], it is suggested that the AB adsorption using diatomite probably involved a chemical mechanism.

3.4. Kinetic Studies. The effect of contact time on the AB adsorption over diatomite at the initial concentrations in the range of 150–900 ppm was presented in Figure 6. It was observed that the amount of AB adsorbed increased from 71 to 140 mg g^{-1} with an increase in the initial AB concentration from 150 to 400 mg L^{-1}. When the initial AB concentration increased from 150 to 400 mg L^{-1}, the adsorption capacity also rose rapidly, thereafter increasing slightly as reaching 400 mg L^{-1}. The reason for this observation might be the increase in initial dye concentration that enhanced the interaction between AB and diatomite. Moreover, the higher initial concentration provides the higher driving force to overcome all the mass transfer resistance of AB between the aqueous solution and the diatomite surface. As a result, high initial AB concentration will enhance the adsorption process [42]. The low adsorption rate at high AB concentration can be explained by the fact that the active sites are sufficient in diatomite surface at low AB/diatomite ratios. However, as AB/diatomite ratio increases, active sites are saturated, leading to a decline in the adsorption efficiency. The equilibrium time was obtained less than 120 minutes at dye concentration from 150 to 900 mg L^{-1}.

In the present paper, the diffusion kinetics was studied by using Webber's model. Because the plots of this model often have a multilinear nature, in general, the graphical method is employed to analyze the data in which the linear segments are determined visually [43]. This method is prone to objectivity. Malash and El-Khaiary [43] suggested a statistical method of piecewise linear regression for the analysis of experimental adsorption data to avoid objective estimation. In this process, the experimental data could be fixed for one, two, or three linear segments' line by Webber's equation:

One linear segment line: $Y = B + AX$ (two parameters),

Two linear segments' line: $Y = B + AX + C * \mathrm{SIGN}(X - D)$ (4 parameters),

Three linear segments' line: $Y = B + AX + C * \mathrm{SIGN}(X - D) + E * \mathrm{SIGN}(X - F)$ (6 parameters),

where the values of A, B, C, D, E, and F are estimated by nonlinear regression. D and F called breakpoints are the boundaries between the segments. The Microsoft Excel "SIGN" function determines the sign of a number and then returns 1 if the number is positive, zero if the number is 0, and −1 if the number is negative. Nonlinear regression estimates the model's parameters by the method of least squares. This is done by minimizing the sum of squared deviations, SSE, by numerical optimization techniques. The function for minimization is

$$\mathrm{SSE} = \sum_{1}^{N} \left(y_{\mathrm{exp}} - y_{\mathrm{est}}\right)^2, \tag{13}$$

where y_{exp} is experimental datum and y_{est} is the valued estimated by model.

It can be clear that the number of parameters, N_p, estimated by nonlinear regression is double the number of linear segments. Increasing the number of regression parameters in model almost universally decreases the sum of squared deviations (SSE) or the coefficient of determination (R^2). Therefore, the goodness of fit cannot be based solely on SSE or R^2 [43]. In other words, SSE or R^2 could not be used to estimate the goodness of fit for two models which have different parameters. In this case, the well-known statistical method used in the comparison of models is based on Akaike's Information Criterion (AIC) [38]. The AICc determines how well the data support each model. The value of AIC can be positive or negative. The model with the lowest AICs score is most likely correct. The AICc (for a small size sample) is calculated for each model from the following equations:

$$\mathrm{AICc} = N \ln\left(\frac{\mathrm{SSE}}{N}\right) + 2N_p + \frac{2N_p\left(N_p + 1\right)}{N - N_p - 1}. \tag{14}$$

The values of AICs calculated by (14) are listed in Table 4. Figure 7, for example, illustrates Webber's plot analyzed by one, two, and three segments' linear regression models for AB adsorption onto diatomite at initial AB concentration of 200 mg L^{-1}. The linear regression for one segment showed poor compatibility with experimental data. The experimental points are distributed very closely to three or segments' linear regression model. Table 4 shows that Webber's model

Table 4: Comparison of models by AICs.

Conc. (mg L^{-1})	Three-segment linear regression			Two-segment linear regression			One-segment linear regression		
	AICc	R^2	SSE	AICc	R^2	SSE	AICc	R^2	SSE
150	−38.718	0.995	2.504	−16.360	0.984	8.252	40.483	0.787	108.878
200	11.765	0.986	20.516	15.272	0.978	30.828	73.675	0.699	434.091
300	41.431	0.980	70.618	35.167	0.980	70.624	49.444	0.955	158.158
400	37.460	0.979	55.772	30.161	0.979	55.732	72.447	0.744	687.983
600	30.006	0.992	37.673	26.661	0.990	46.358	89.127	0.726	1241.451
800	43.545	0.976	76.824	50.517	0.961	162.706	87.642	0.515	1530.680
900	33.916	0.981	46.283	76.460	0.743	637.383	102.018	0.644	881.597

Table 5: Results of piecewise linear regression for the three linear segments in the Webber plots for different initial concentration. The values in parentheses are 95% confidence limits.

Conc. (mg L^{-1})	First-segment linear line		Second-segment linear line		Third-segment linear line	
	I_1 (min^{-1})	k_{1i} (mg g^{-1} min^{-1})	I_2 (min^{-1})	k_{2i} (mg g^{-1} min^{-1})	I_3 (min^{-1})	k_{3i} (mg g^{-1} min^{-1})
150	53.44 (50.05–56.82)	3.78	60.18 (58.94–61.43)	1.16	68.70 (68.07–69.33)	0.16
200	55.26 (42.42–68.10)	11.23	78.44 (76.76–80.10)	1.469	89.05 (88.02–90.08)	0.28
300	86.10 (83.23–88.96)	4.84	85.29 (83.00–87.59)	5.11	97.24 (94.52–99.96)	1.58
400	81.30 (68.15–94.46)	14.95	97.46 (94.64–100.31)	6.71	127.03 (124.37–129.68)	0.75
600	94.53 (86.89–102.17)	2.971	122.24 (118.06–126.43)	1.47	91.22 (88.23–94.22)	7.80
800	78.46 (60.58–96.34)	19.75	110.82 (107.28–114.35)	6.02	142.53 (138.00–147.06)	0.14
900	79.45 (70.69–88.22)	16.18	100.26 (97.24–103.28)	6.819	127.32 (122.86–131.76)	0.63

analyzed three segments' linear regression provides the lowest AICc in comparison with one or two segment models. In conclusion, the experimental data were best fit with the three segments linear regression model.

Results of piecewise linear regression for different initial concentration were obtained from Table 5. For example, for 200 mg L^{-1} concentration it was found that the intercept of the first, second, and third linear segment lines in the Webber plot was 55.26 with 95% confidence limits of 42.42 to 68.10; 78.44 with 95% confidence limits of 76.76–80.10; 89.05 with 95% confidence limits of 88.02–90.08, respectively. This value of the intercept was significantly different from zero. It means the line did not pass through the origin. The similar behaviors were observed for all the other cases. Moreover the intraparticle parameters illustrated in Table 3 show that k_1 value is irregular as initial AB concentration increases. These results strongly suggest that the AB adsorption on diatomite is controlled by film diffusion or chemical reaction controls the adsorption rate (e.g., surface adsorption and liquid film diffusion) instead of intraparticle diffusion [19, 43]. From Figure 7 the breakpoints for first and second period time are 2.6 and 8.9 min, respectively. They are corresponding to the time where the transition of adsorption stage could occur. It is clear that the curves in Figure 6 presented three distinct stages: (i) immediate adsorption of AB molecules within 2.6 min of the contact times, (ii) gradual attainment of the equilibrium where only about 5–10% of the adsorption is encountered; this is due to the utilization of the all active sites on the adsorbent surface, and (iii) an equilibrium attainment of AB molecules onto diatomite. The same behaviors for other concentration were also observed. It is emphasized that analysis of experimental adsorption data by using piecewise linear regression for Webber's intraparticle-diffusion models is useful for providing the exact time periods for each diffusion.

In order to determine the rate-limiting step, kinetic models such as *pseudo*-first-order and *pseudo*-second-order equation were employed to evaluate the experimental data. The parameters of kinetics equations (7) and (8) obtained by nonlinear regression method were listed in Table 6. R^2 could be used to compare *pseudo*-first-order and *pseudo*-second-order models for the goodness of fit because both models have the same parameters and experimental points. For initial concentration from 200 to 400 the experimental points of the *pseudo*-second-order kinetic model reflected high correlation coefficients (R^2 = 0.804–0.999) and $q_{e,\mathrm{cal}}$

Table 6: Kinetic parameters of *pseudo*-first- and second-order kinetic model.

Initial conc. ($mg\,L^{-1}$)	*Pseudo*-first-order kinetic model			*Pseudo*-second-order kinetic model			
	k_1 (min^{-1})	R^2	$q_{e,cal}$ ($mg\,g^{-1}$)	k_2 ($mg\,g^{-1}\,min^{-1}$)	R^2	$q_{e,cal}$ ($mg\,g^{-1}$)	$q_{e,exp}$ ($mg\,g^{-1}$)
150	1.620	0.252	66.99	0.041	0.999	69.10	71.2
200	1.040	0.487	87.69	0.020	0.980	91.10	93.0
300	1.370	0.133	109.63	0.016	0.994	114.86	133.2
400	1.130	0.389	124.07	0.014	0.811	130.78	136.6
600	0.790	0.990	124.08	0.009	0.804	132.72	140.0
800	0.943	0.995	133.69	0.012	0.875	140.32	141.1
900	1.100	0.996	124.60	0.015	0.871	130.39	135.2

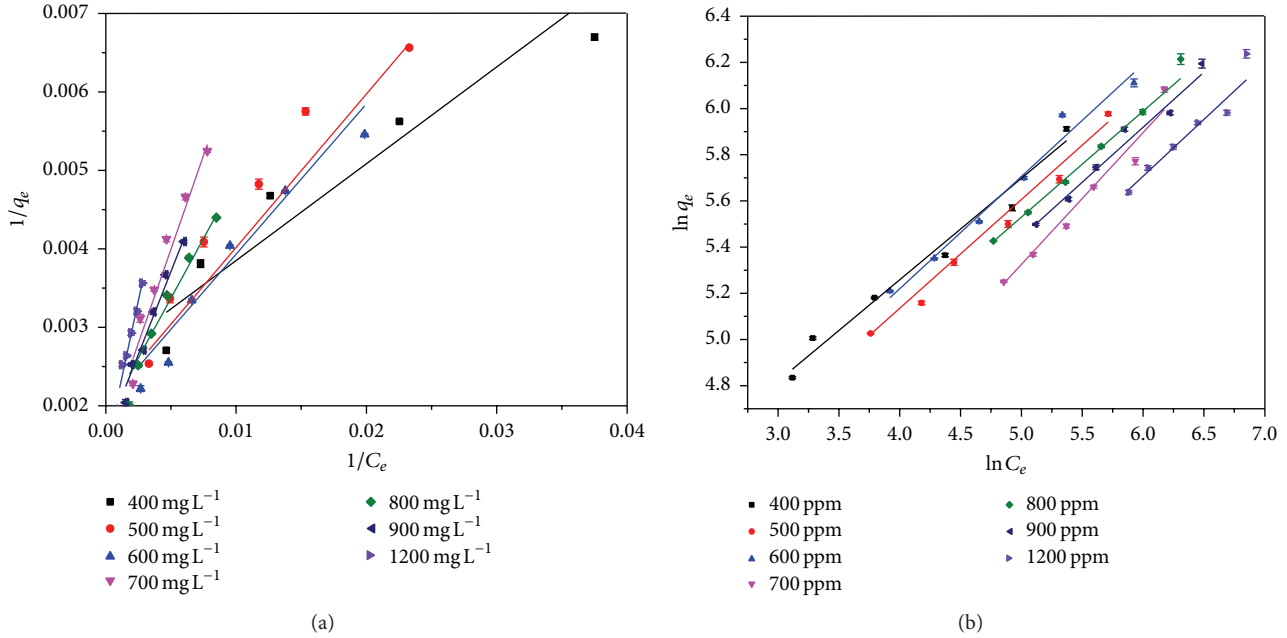

Figure 4: Plots of Langmuir (a) and Freundlich (b) adsorption isotherms for AB/diatomite system: adsorption condition: mass of adsorbent = 50; 100; 150; 200; 250; and 300 mg, volume of solution = 100 mL, equilibrium time = 24 h, temperature = 25 ± 1°C, and pH of dyes solution = 7.0.

values agreed with the value $q_{e,exp}$ indicating that the adsorption may be governed by a *pseudo*-second-order mechanism. This suggests that the rate-limiting step is a chemical adsorption which might be involved in the formation of covalent bonds between AB molecules and diatomite through enabled sharing or exchange of electrons. A chemisorption mechanism only allows for a monolayer adsorption, which is in good agreement with Langmuir model that describes well the equilibrium adsorption data [44]. The *pseudo*-second-order kinetic rate coefficient decreases from 0.040 to 0.009 $mg\,g^{-1}\,min^{-1}$ when the initial AB concentration increases from 150 to 600 $mg\,L^{-1}$. This behavior was observed by various authors [37, 44]. This could be attributed to the fact that increasing the dye concentration might reduce the diffusion of dye molecules in the boundary layer and enhance the diffusion in the solid [37]. Conversely, high correlation (R^2 = 0.990–0.996) with the *pseudo* first order was observed at higher initial concentration in the range of 600–900 $mg\,L^{-1}$ indicating that the AB adsorption process obeys the *pseudo*-first-order kinetic model. At high concentration possible desorption might be occurring where the AB adsorption capacity appears to fluctuate or even reduce as little as shown in Figure 4. This behavior could be attributed to either a reversible adsorption or a back diffusion controlling mechanism [28, 45] indicating that rate-limiting step in this case involved a physical-chemical mechanism and not purely physical or chemical.

4. Conclusions

The Vietnamese diatomite, which is composed of amorphous silica, has high porosity and surface area. It was studied as an adsorbent for the removal of AB dye from aqueous solution. Solution pH has a significant influence in the adsorption of AB, where the capacity of the adsorbents increases with increasing pH from 4.0 to 11.0. Experimental isothermal data were fitted well to both Langmuir and Freundlich model in the large range of 400–1400 $mg\,L^{-1}$. The maximum adsorption capacity, q_m = 518.0 ± 13.2 $mg\,g^{-1}$, calculated from Freundlich equation and q_{mom} = 528 ± 62 $mg{\cdot}g^{-1}$ calculated

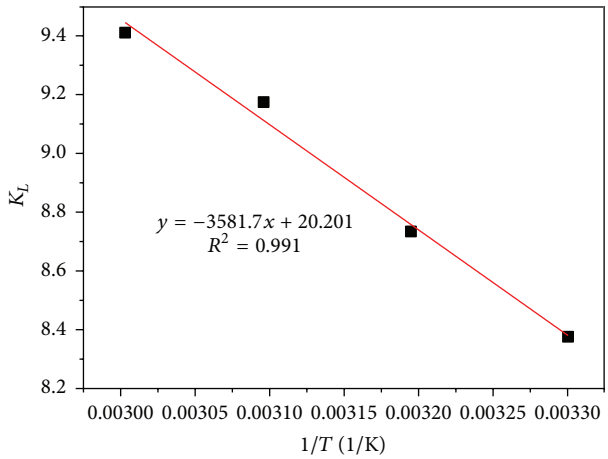

Figure 5: Van't Hoff's plot for AB adsorption onto diatomite: experimental variables: mass of adsorbent = 50, 100, 150, 200, 250, and 300 mg, initial concentration = 300 mg L^{-1}, adsorption temperature = 303, 313, 323, 333, and 343 K, volume of solution = 100 mL, equilibrium time = 200 min, and pH of dyes solution = 7.

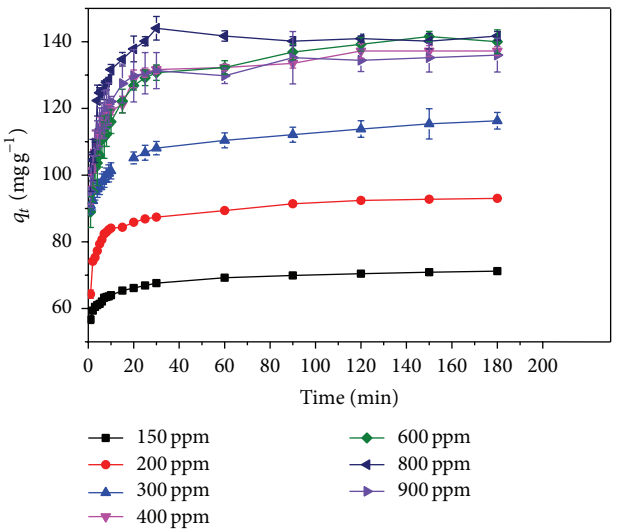

Figure 6: Effect of initial dye concentration on the adsorption of AB at 25°C. Adsorption condition: initial AB concentration: 150–900 mg L^{-1}, temperature = 25 ± 1°C, mass of adsorbent = 2.0 g, volume of solution = 1000 mL, stirring speed = 300 rpm, and pH of dyes solution = 7.

from Langmuir equation, is statistically similar. However, parameters of these equations had an effect remarkably on the initial AB concentrations. Both values of q_{mom} and q_m increase with the increasing initial AB concentration. The free energy of AB adsorption on diatomite is more negative at higher temperature, which demonstrates that the spontaneity increases with the rise of temperature. Piecewise linear regression as a statistical method for the analysis of experimental adsorption data by Webber's intraparticle-diffusion models provides the time periods for each diffusion and results show that the AB adsorption onto diatomite was film diffusion controlled. The rate-limiting step has effect

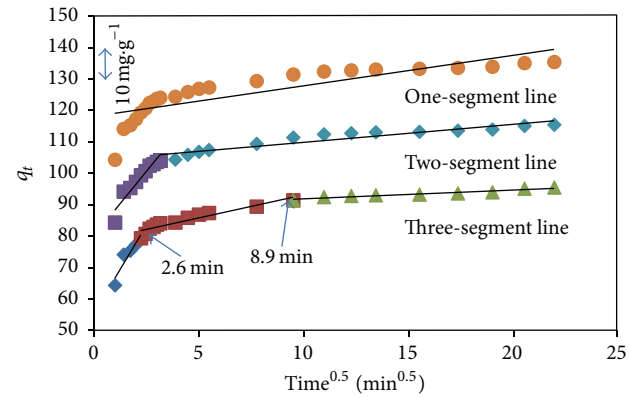

Figure 7: Plot of piecewise linear regression for one, two, and three segments in the Webber plot. Experimental condition: initial AB concentration: 200 mg L^{-1}, mass of diatomite: 2.0 g, and temperature: 25 ± 1°C.

on the initial AB concentration. The adsorption processes obey the *pseudo*-second-order process in the range of 150–400 mg L^{-1} and the *pseudo*-first-order one in range of 400–900 mg L^{-1}.

Competing Interests

The authors declare that they have no competing interests.

References

[1] B. Kayan, B. Gözmen, M. Demirel, and A. M. Gizir, "Degradation of acid red 97 dye in aqueous medium using wet oxidation and electro-Fenton techniques," *Journal of Hazardous Materials*, vol. 177, no. 1-3, pp. 95–102, 2010.

[2] V. K. Gupta and Suhas, "Application of low-cost adsorbents for dye removal—a review," *Journal of Environmental Management*, vol. 90, no. 8, pp. 2313–2342, 2009.

[3] F. A. Pavan, Y. Gushikem, A. C. Mazzocato, S. L. P. Dias, and E. C. Lima, "Statistical design of experiments as a tool for optimizing the batch conditions to methylene blue biosorption on yellow passion fruit and mandarin peels," *Dyes and Pigments*, vol. 72, no. 2, pp. 256–266, 2007.

[4] B. Royer, E. C. Lima, N. F. Cardoso, T. Calvete, and R. E. Bruns, "Statistical design of experiments for optimization of batch adsorption conditions for removal of reactive red 194 textile dye from aqueous effluents," *Chemical Engineering Communications*, vol. 197, no. 5, pp. 775–790, 2010.

[5] G. M. Walker and L. R. Weatherley, "Biodegradation and biosorption of acid anthraquinone dye," *Environmental Pollution*, vol. 108, no. 2, pp. 219–223, 2000.

[6] M. Zhou and J. He, "Degradation of azo dye by three clean advanced oxidation processes: wet oxidation, electrochemical oxidation and wet electrochemical oxidation—a comparative study," *Electrochimica Acta*, vol. 53, no. 4, pp. 1902–1910, 2007.

[7] M. H. V. Baouab, R. Gauthier, H. Gauthier, B. Chabert, and E. B. Rammah, "Immobilization of residual dyes onto ion-exchanger cellulosic materials," *Journal of Applied Polymer Science*, vol. 77, no. 1, pp. 171–183, 2000.

[8] Y. Xu, R. E. Lebrun, P.-J. Gallo, and P. Blond, "Treatment of textile dye plant effluent by nanofiltration membrane," *Separation Science and Technology*, vol. 34, no. 13, pp. 2501–2519, 1999.

[9] P. Peralta-Zamora, A. Kunz, S. Gomes de Moraes et al., "Degradation of reactive dyes I. A comparative study of ozonation, enzymatic and photochemical processes," *Chemosphere*, vol. 38, no. 4, pp. 835–852, 1999.

[10] M. Koch, A. Yediler, D. Lienert, G. Insel, and A. Kettrup, "Ozonation of hydrolyzed azo dye reactive yellow 84 (CI)," *Chemosphere*, vol. 46, no. 1, pp. 109–113, 2002.

[11] Y. Yang, D. T. Wyatt II, and M. Bahorsky, "Decolorization of dyes using UV/H_2O_2 photochemical oxidation," *Textile Chemist and Colorist*, vol. 30, no. 4, pp. 27–35, 1998.

[12] R. Pelegrini, P. Peralta-Zamora, A. R. De Andrade, J. Reyes, and N. Durán, "Electrochemically assisted photocatalytic degradation of reactive dyes," *Applied Catalysis B: Environmental*, vol. 22, no. 2, pp. 83–90, 1999.

[13] A. A. Attia, B. S. Girgis, and N. A. Fathy, "Removal of methylene blue by carbons derived from peach stones by H_3PO_4 activation: batch and column studies," *Dyes and Pigments*, vol. 76, no. 1, pp. 282–289, 2008.

[14] A. A. Adeyemo, I. O. Adeoye, and O. S. Bello, "Adsorption of dyes using different types of clay: a review," *Applied Water Science*, vol. 20, no. 2, pp. 1–26, 2015.

[15] D. Sun, X. Zhang, Y. Wu, and X. Liu, "Adsorption of anionic dyes from aqueous solution on fly ash," *Journal of Hazardous Materials*, vol. 181, no. 1–3, pp. 335–342, 2010.

[16] D. Karadag, E. Akgul, S. Tok, F. Erturk, M. A. Kaya, and M. Turan, "Basic and reactive dye removal using natural and modified zeolites," *Journal of Chemical and Engineering Data*, vol. 52, no. 6, pp. 2436–2441, 2007.

[17] G. Sheng, J. Hu, and X. Wang, "Sorption properties of Th(IV) on the raw diatomite-effects of contact time, pH, ionic strength and temperature," *Applied Radiation and Isotopes*, vol. 66, no. 10, pp. 1313–1320, 2008.

[18] H. Zaitan and T. Chafik, "FTIR determination of adsorption characteristics for volatile organic compounds removal on diatomite mineral compared to commercial silica," *Comptes Rendus Chimie*, vol. 8, no. 9-10, pp. 1701–1708, 2005.

[19] M. A. Al-Ghouti, M. A. M. Khraisheh, M. N. M. Ahmad, and S. Allen, "Adsorption behaviour of methylene blue onto Jordanian diatomite: a kinetic study," *Journal of Hazardous Materials*, vol. 165, no. 1–3, pp. 589–598, 2009.

[20] E. Erdem, G. Çölgeçen, and R. Donat, "The removal of textile dyes by diatomite earth," *Journal of Colloid and Interface Science*, vol. 282, no. 2, pp. 314–319, 2005.

[21] E. Haque, V. Minett, A. I. Lo, A. T. Harrisa, and T. L. Church, "Dichotomous adsorption behavious of dyes on an amino-funtionalised metal-organic framwork, amino MIL-101(Al)," *Journal of Materials Chemistry A*, vol. 2, no. 1, pp. 193–203, 2014.

[22] I. Langmuir, "The constitution and fundamental properties of solids and liquids. Part I. Solids," *The Journal of the American Chemical Society*, vol. 38, no. 2, pp. 2221–2295, 1916.

[23] M. Irani, M. Amjadi, and M. A. Mousavian, "Comparative study of lead sorption onto natural perlite, dolomite and diatomite," *Chemical Engineering Journal*, vol. 178, pp. 317–323, 2011.

[24] H. M. F. Freundlich, "Over the adsorption in solution," *Journal of Physical Chemistry*, vol. 57, no. 25, pp. 385–471, 1906.

[25] S. Ma, J. Zhang, D. Sun, and G. Liu, "Surface complexation modeling calculation of Pb(II) adsorption onto the calcined diatomite," *Applied Surface Science*, vol. 359, pp. 48–54, 2015.

[26] D. Mohan, V. K. Gupta, S. K. Srivastava, and S. Chander, "Kinetics of mercury adsorption from wastewater using activated carbon derived from fertilizer waste," *Colloids and Surfaces A: Physicochemical and Engineering Aspects*, vol. 177, no. 2-3, pp. 169–181, 2001.

[27] A. Sivasamy, K. P. Singh, D. Mohan, and M. Maruthamuthu, "Studies on defluoridation of water by coal-based sorbents," *Journal of Chemical Technology and Biotechnology*, vol. 76, no. 7, pp. 717–722, 2001.

[28] M. Al-Ghouti, M. A. M. Khraisheh, S. J. Allen, and M. N. Ahmad, "Thermodynamic behaviour and the effect of temperature on the removal of dyes from aqueous solution using modified diatomite: a kinetic study," *Journal of Colloid and Interface Science*, vol. 287, no. 1, pp. 6–13, 2005.

[29] K. V. Kumar and S. Sivanesan, "Pseudo second order kinetic models for safranin onto rice husk: comparison of linear and non-linear regression analysis," *Process Biochemistry*, vol. 41, no. 5, pp. 1198–1202, 2006.

[30] W. J. Weber and J. C. Morris, "Kinetics of adsorption on carbon from solution," *Journal of the Sanitary Engineering Division—Civil Engineering*, vol. 89, no. 2, pp. 31–59, 1963.

[31] E. G. Vrieling, T. P. M. Beelen, R. A. Van Santen, and W. W. C. Gieskes, "Mesophases of (bio)polymer-silica particles inspire a model for silica biomineralization in diatoms," *Angewandte Chemie—International Edition*, vol. 41, no. 9, pp. 1543–1546, 2002.

[32] T. Wajima, M. Haga, K. Kuzawa et al., "Zeolite synthesis from paper sludge ash at low temperature (90 °C) with addition of diatomite," *Journal of Hazardous Materials*, vol. 132, no. 2-3, pp. 244–252, 2006.

[33] G. Rytwo, D. Tropp, and C. Serban, "Adsorption of diquat, paraquat and methyl green on sepiolite: experimental results and model calculations," *Applied Clay Science*, vol. 20, no. 6, pp. 273–282, 2002.

[34] S. Hayakawa and L. L. Hench, "AMI study on infra-red spectra of silica clusters modified by fluorine," *Journal of Non-Crystalline Solids*, vol. 262, no. 1–3, pp. 264–270, 2000.

[35] P. Yuan, D. Q. Wu, H. P. He, and Z. Y. Lin, "The hydroxyl species and acid sites on diatomite surface: a combined IR and Raman study," *Applied Surface Science*, vol. 227, no. 1–4, pp. 30–39, 2004.

[36] Y. Du, G. Zheng, J. Wang, L. Wang, J. Wu, and H. Dai, "MnO_2 nanowires in situ grown on diatomite: highly efficient absorbents for the removal of Cr(VI) and As(V)," *Microporous and Mesoporous Materials*, vol. 200, pp. 27–34, 2014.

[37] M. A. Al-Ghouti, M. A. M. Khraisheh, M. N. M. Ahmad, and S. Allen, "Adsorption behaviour of methylene blue onto Jordanian diatomite: a kinetic study," *Journal of Hazardous Materials*, vol. 165, no. 1—3, pp. 589–598, 2009.

[38] G. D. Halsey, "The role of surface heterogeneity in adsorption," *Advances in Catalysis*, vol. 4, pp. 259–269, 1952.

[39] H. Motulsky and A. Christopoulos, *Fitting Models to Biological Data Using Linear and Non-Linear Regression*, GraphPad Software, San Diego, Calif, USA, 2003, http://www.graphpad.com.

[40] E. I. Unuabonah, K. O. Adebowale, and B. I. Olu-Owolabi, "Kinetic and thermodynamic studies of the adsorption of lead (II) ions onto phosphate-modified kaolinite clay," *Journal of Hazardous Materials*, vol. 144, no. 1-2, pp. 386–395, 2007.

[41] J. M. Smith, *Chemical Engineering Kinetics*, McGraw Hill Book Company, New York, NY, USA, 3rd edition, 1982.

[42] V. Vadivelan and K. Vasanth Kumar, "Equilibrium, kinetics, mechanism, and process design for the sorption of methylene

blue onto rice husk," *Journal of Colloid and Interface Science*, vol. 286, no. 1, pp. 90–100, 2005.

[43] G. F. Malash and M. I. El-Khaiary, "Piecewise linear regression: a statistical method for the analysis of experimental adsorption data by the intraparticle-diffusion models," *Chemical Engineering Journal*, vol. 163, no. 3, pp. 256–263, 2010.

[44] C.-C. Kan, M. C. Aganon, C. M. Futalan, and M. L. P. Dalida, "Adsorption of Mn^{2+} from aqueous solution using Fe and Mn oxide-coated sand," *Journal of Environmental Sciences*, vol. 25, no. 7, pp. 1483–1491, 2013.

[45] N. K. Lazaridis, T. D. Karapantsios, and D. Georgantas, "Kinetic analysis for the removal of a reactive dye from aqueous solution onto hydrotalcite by adsorption," *Water Research*, vol. 37, no. 12, pp. 3023–3033, 2003.